# Dynamic Control of Soft Robotic Arm: An Experimental Study

Milad Azizkhani, Student Member, IEEE, Anthony L. Gunderman, Student Member, IEEE, Isuru S. Godage, Member, IEEE, and Yue Chen, Member, IEEE

Abstract—The objective of this letter is to investigate the dynamic control of a soft robotic arm. First, a modular soft robotic hardware and an affordable actuator-space encoder were presented. We then discussed the soft robot modeling, and adaptive passivity control strategy with stability proof. The proposed controller was tested in different operation scenarios, and compared to the standard PD feedback linearization control and passivity control. In all experimental settings, the adaptive passivity control scheme was able to achieve superior performance, even with significant modeling uncertainties and disturbances. The theoretical analysis and experimental validations of the proposed controller will pave the way toward the practical implementations of the soft robotic system in the dynamic scenarios.

Index Terms—Soft robot, dynamics, adaptive control.

#### I. INTRODUCTION

OFT robots, inspired by nature, have been introduced to the robotics community to provide abilities that can surpass their rigid counterparts [1]. These robots are made from inherently elastic materials such as silicone or rubber, emulating biological structures while improving robot safety and compliance [2]. They can be considered as the infinite degree of freedom systems due to the elastic materials, which can present different adaptive, agile motions ranging from elongation, twisting, bending, etc. [3]. These behaviors make soft robots an ideal tool for different applications, including grasping [4], [5], medical procedures [6], [7], rehabilitation [8], agricultural harvesting [9], snake locomotion [10], etc. Among them, manipulation has often been considered one of the most important robotic applications. Despite much progress have been made in the past 20 years, controlling these soft robots to achieve desired tracking performance in dynamic operation scenarios remains challenging [11].

Manuscript received 15 September 2022; accepted 22 January 2023. Date of publication 10 February 2023; date of current version 20 February 2023. This letter was recommended for publication by Associate Editor C. Della Santina and Editor C. Gosselin upon evaluation of the reviewers' comments. This work was supported by the Georgia Tech IRIM seed. (Corresponding author: Yue Chen.)

Milad Azizkhani and Anthony L. Gunderman are with the Georgia Tech Institute for Robotics and Intelligent Machines, Atlanta, GA 30313 USA (e-mail: mazizkhani3@gatech.edu; agunderman3@gatech.edu).

Yue Chen is with the Georgia Tech Institute for Robotics and Intelligent Machines, Atlanta, GA 30313 USA, and also with the Department of Biomedical Engineering, Georgia Tech/Emory, Atlanta, GA 30313 USA (e-mail: yue.chen@bme.gatech.edu).

Isuru S. Godage is with the Engineering Technology and Industrial Distribution, Texas A&M University, College Station, TX 77843 USA (e-mail: igodage@tamu.edu).

This letter has supplementary downloadable material available at https://doi.org/10.1109/LRA.2023.3243802, provided by the authors.

Digital Object Identifier 10.1109/LRA.2023.3243802

Generally, model-based control has been the predilection of robotics researchers for dynamic control due to the availability of stability proofs. However, the primary limitation is the requirement of accurate system model in order to cancel out the dynamics. Accurate modeling in soft robots can be achieved using Cosserat rod theory [12], [13] and finite element methods [14], but both have the limitation of real-time implementation in the complicated soft robotic systems due to their computationally expensive calculations [15]. Several groups have been addressing these problems by proposing modified approaches, but still, their real-time implementations in complicated robotic systems are understudied [16]. Another approach is to use simplified assumptions, for example, lumped parameter models, derived from the piece-wise constant curvature (PCC) assumption and Euler-Lagrange formulations can be considered as suitable candidates for real-time implementations [17], [18]. However, lumped parameter models are susceptible to uncertainties that limit accuracy and applicability. To resolve this issue, a robust control algorithm that can address unknown factors is required to achieve the desired performance.

There is an ongoing trend to explore advanced control strategies for uncertainty compensation in soft robots. Azizkhani et al. [19] considered the dynamics of a 1-DOF soft robot actuator as a second-order model while the variation in system parameters along with unknown dynamics and external disturbances were compensated with a robust model reference adaptive controller. Godage et al. [20] modeled the system dynamics as a second-order system with hysteresis and used it to cancel out the dynamics, while the remaining effects were compensated by a PID controller. In another study [21], a nonlinear controller with unscented Kalman filter and feedback linearization was used to control a bending actuator. In our previous study [22], we have shown that an adaptive passivity control with sigma modification can handle parametric uncertainty, external disturbances, payloads, sensor noise, and achieve fast tracking with improved performance compared to the conventional PD Feedback linearization [23], [24]. Other studies have also demonstrated the use of adaptive controllers to address the uncertainties and unknown dynamics in soft robotic arms, such as implementing adaptive control [25] inspired by [26], and adaptive terminal sliding mode control [27] to improve convergence speed. However, fast and dynamic robot trajectory tracking on physical hardware is still lacking. For example, Falkenhahn et al. [24] focused on set-point tracking instead of trajectory tracking. In [27], trapezoidal paths were used for robot tracking with a maximum speed and acceleration of 0.11 m/sec and 0.05 m/sec<sup>2</sup>, respectively.

In this letter, we build upon our prior work [22] by implementing the proposed controller on a soft robotic arm, enabling

2377-3766 © 2023 IEEE. Personal use is permitted, but republication/redistribution requires IEEE permission. See https://www.ieee.org/publications/rights/index.html for more information.

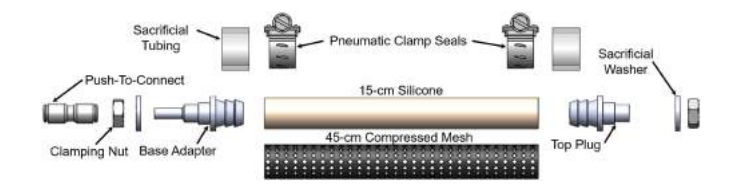


Fig. 1. Exploded view of the soft robotic actuator.

tracking speeds and accelerations of up to 0.15 m/sec and 0.45 m/sec<sup>2</sup>, respectively. We provide four contributions in this letter: (1) incorporation of an affordable actuator-space encoder, eliminating the need for observer-based velocity measurements in the actuator space, (2) derivation of the stability proof, including signal boundedness and error convergence of the closed system, (3) investigation of the dynamic tracking of the adaptive passivity controller, and (4) compensation of disturbances and uncertainties in challenging scenarios during trajectory tracking. By investigating the advantages and limitations of the proposed controller, we aim to pave the road for versatile soft robotic manipulation in practical applications, such as harvesting or food automation. The rest of the letter is organized as follows. Section II presents the hardware design. Section III briefly reviews the kinematic and dynamic model. Section IV briefly reviews PD feedback linearizaton, and passivity control, and primarily focuses on the controller derivation and stability proof of the adaptive passivity controller. In Section V, the system experimental results and discussions are provided. The letter is concluded in Section VI.

### II. HARDWARE DESIGN

In this section, we aim to provide a modular, affordable soft robotic arm design by detailing the fabrication process and item number for both the soft actuator and encoder unit, respectively.

#### A. Soft Actuator Design

The elongation actuator consists of a 15 cm silicone rubber segment (4G-60518-latex tube, Feelers, USA) surrounded by a 45 cm mesh (B00ZCNTIRQ, Electriduct, USA) (Fig. 1). The silicone segment has an inner diameter of 12 mm and an outer diameter of 17 mm. The mesh has a width (prior to compression) of 5/8". The length pair with these dimensions results in a 65% potential elongation. The silicone segment is cut using standard scissors; however, the mesh segment is cut to length using a soldering station (5040-XR3, X-TRONIC, USA) to prevent fraying at the mesh ends. A custom-designed plug has been developed for both the distal and proximal end of the actuator to provide a modular attachment method to the base of the soft robot section. The plug is manufactured using a stereolithography (SLA) printer (Form 3B, Formlabs, USA) to provide an air-tight seal. Two clamps (B078BRJK8Z, LOKMAN, China) are used at both ends to prevent air leakage. Sacrificial tubing (Z20210816W25, VictorsHome, USA) is used between the elongating mesh and the clamps to mitigate the risk of tearing due to the metal clamps and large moments existing at the base of the silicone rubber. Clamping nuts and washers are used to connect the actuator to the main plates of the soft robot section (Fig. 2).

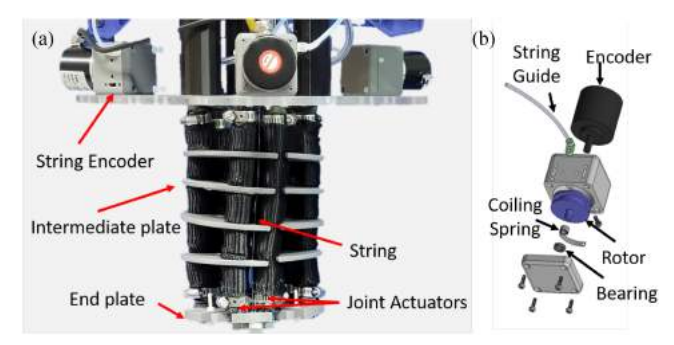


Fig. 2. (a) 3-DoF soft robot prototype along with (b) the proposed string encoders for actuator-space measurements.

To enhance the robot stiffness for high-payload applications, two actuators have been placed in parallel to create a reinforced elongation actuator, a distinct difference from our prior work [22]. The placement of each actuator pair is 120 degrees apart around the central axis. Note that their inlets are connected via a T-shape fitting. This enables identical joint elongation with significantly increased stiffness, allowing for quick customization for different application requirements. As can be seen in Fig. 2, four intermediate plates have been used to constrain the robot to allow applicability of the piece-wise constant curvature (PCC) assumption.

#### B. Encoder Design

The kinematic variables of a soft robotic arm are defined by the length change of each actuator. Measurement of the actuator-space variables can be obtained using the string encoders [Fig. 2(b)]. In this letter, we present a custom-designed string encoder developed based on the standard quadrature encoder (B07MX1SYXB, Taiss, China). Although off-the-shelf string encoders exist, developing our own encoder improves affordability and enables compact packaging with the proposed soft robotic system. The quadrature encoder is attached to a 3-D printed housing that contains a 3-D printed spool with a monofilament string (BGQS30C-15, Berkley, USA). The spool is attached to the assembly in two ways: (i) directly attached to the quadrature encoder via a keyed shaft, and (ii) to the housing via a rotary spring (9293K112, McMaster, USA). Thus, the spool directly drives the encoder when the monofilament string is pulled, and the rotary spring returns the spool to the starting position when the monofilament string is released. The rotatory quadrature encoder provides a resolution of 600 pulses per revolution, resulting in a 0.03 mm linear resolution when coupled with the spool. Using basic geometry knowledge, the relation between elongation and encoder output is described as follows:

$$\Delta l = \frac{2\pi r_e}{4n} p \tag{1}$$

where  $r_e$  is the radius of the encoder rotor, n is the number of pulses per revolution, 4 is for quadrature reading of the encoder, and p is the input pulse. Thus, the actuator elongation can be obtained when the monofilament string is routed through holes in the proximal, distal, and intermediate plates with a fixed offset from the soft actuators.

#### III. SYSTEM MODELING

#### A. Kinematic Modeling

In this section, we briefly review the kinematic modeling of the soft robotic arm based on [22], [28]. To define the robot's position in 3D space, two mappings have been used: (i) actuator space to configuration space, and (ii) configuration space to task space.

1) Actuator Space to Configuration Space: To define the relationship between actuator variables to configuration variables, the length of actuators is considered as follows

$$L_i(t) = L_0 + l_i(t) \tag{2}$$

where  $L_i$  represents the  $i^{th}$  actuator total length,  $L_0$  is the initial length, and  $l_i$  is the  $i^{th}$  actuator elongation. The actuator variables vector is represented by  $\mathbf{q} = [l_1, l_2, l_3]^T$  and  $\mathbf{q} \in \mathbb{R}^3$ . The mapping is derived based on the geometrical location of the actuators (120 degrees apart with a constant radius from the base center) and PCC assumption as follows

$$s = \sqrt{l_1^2 + l_2^2 + l_3^2 - l_1 l_2 - l_2 l_3 - l_1 l_3}, \ \phi = \frac{2 s}{3 r_k}$$

$$\lambda = \frac{(3L_0 + l_1 + l_2 + l_3) r_k}{2 s}, \ \theta = \arctan\left(\frac{\sqrt{3}(l_3 - l_2)}{l_2 + l_3 - 2l_1}\right)$$
(3)

where  $\phi \in [0, 2\pi)$  is the bending angle of the arc,  $\lambda \in (0, \infty)$  is the radius of the curvature,  $\theta \in [-\pi, \pi]$  is the bending angle with respect to the X-Axis, and  $r_k$  is the distance of actuators from the center of plate (46.32 mm in this work).

2) Configuration Space to Task Space: The homogeneous transformation  $T \in SE(3)$  is defined as follows:

$$T(\xi, \boldsymbol{q}) = \text{Rot}_z(\theta) \text{Trans}_x(\lambda) \text{Rot}_y(\xi\phi) \text{Trans}_x(-\lambda) \text{Rot}_z(-\theta)$$
(4)

where  $\operatorname{Rot}_{\gamma}$  and  $\operatorname{Trans}_{\gamma}$  define a homogeneous transformation in SE(3) for rotation around  $\gamma$  axis and translation along  $\gamma$  axis, respectively.  $\xi \in [0,1]$  is an auxiliary variable that defines an imaginary disk between the proximal  $(\xi=0)$  and distal end  $(\xi=1)$ .

#### B. Dynamic Modeling

The dynamic model of the robot can be derived using the Euler-Lagrange formulation [17], [22]

$$M\ddot{\mathbf{q}} + C\dot{\mathbf{q}} + D\dot{\mathbf{q}} + K\mathbf{q} + \mathbf{G} + \mathbf{H} = J^T \mathbf{F}_{ext} + \boldsymbol{\tau}$$
 (5)

where M represents the inertia matrix, C represents centrifugal and Coriolis force matrix, D represents the damping force matrix, K represents the stiffness matrix of the system, G is the gravitational force matrix, and H represents hysteresis behavior.  $F_{ext}$  represents external forces, J is the Jacobian of the system with respect to the base frame, and  $\tau$  is the resulting forces from input pressure acting upon the actuators.

The inertia matrix is calculated as

$$M = M^w + M^v \tag{6}$$

where  $M^w$  and  $M^v$  are generalized angular and linear inertia matrices and are derived as follows

$$M^w[j,k] = I_{xx} \int_{\xi} \mathbb{T}_2 \left[ \left( \frac{\partial R}{\partial q(j)} \right) \left( \frac{\partial R}{\partial q(k)} \right) \right]$$

$$M^{v}[j,k] = m \int_{\mathcal{E}} \left( \frac{\partial \mathbf{P}}{\partial q(j)} \right) \left( \frac{\partial \mathbf{P}}{\partial q(k)} \right)$$
 (7)

where  $R \in SO(3)$  represents the rotation matrix and  $P \in \mathbb{R}^3$  is the position of the robot, which is a function of  $\xi$  that describes all nodes from the proximal to the distal end of the robot.  $\mathbb{T}_2$  is an operator which sums the first two elements of the principal diagonal  $\mathbb{R}^{3\times3}$  matrix. m is the mass of the continuum section and  $I_{xx}$  is the moment of inertia and is derived as  $I_{xx} = \frac{1}{4}mr_k^2$  [18].

The centrifugal and Coriolis matrix is defined as follows

$$C[k,j] = \sum_{i=1}^{3} \Gamma_{ijk}(M)\dot{q}(i)$$

$$\Gamma_{ijk}(M) = \frac{1}{2} \left( \frac{\partial M[k,j]}{\partial q(i)} + \frac{\partial M[k,i]}{\partial q(j)} - \frac{\partial M[i,j]}{\partial q(k)} \right)$$
(8)

where  $i, j, k \in \{1, 2, 3\}$  are placeholders that represent the index for actuator variables.

Furthermore, the gravitational forces are derived as

$$G(i) = m \int_{\mathcal{E}} J^{vT}(i) R^T \mathbf{G}_{v}$$
 (9)

where  $G_v = [0, 0, g]^T$ ,  $i \in \{1, 2, 3\}$ , and  $J^v$  is the Jacobian of the moving frame.

It should be noted that the hysteresis behavior is an inherent characteristic of soft robotic systems. In this study, we will use the Bouc-Wen model [29] to describe the hysteresis as follows

$$\dot{h}_i = q(i) \left[ \alpha_h - \left\{ \beta_h \operatorname{sgn}(\dot{q}(i)h_i) + \gamma_h \right\} |h_i| \right] \tag{10}$$

where  $\alpha_h$ ,  $\beta_h$ ,  $\gamma_h$  are the constant parameters of the model and  $\boldsymbol{H} = [h_1, h_2, h_3]^T$  in (5).

#### IV. DYNAMIC CONTROLLER DESIGN

#### A. Proposed Control: Adaptive Passivity (AP) Control

To compensate for the modeling uncertainties and external disturbances, we will propose the adaptive passivity controller here [22], [30], as detailed below

$$v = \dot{q}_d - \Lambda \tilde{q}, a = \dot{v} = \ddot{q}_d - \Lambda \dot{\tilde{q}}, r = \dot{q} - v = \dot{\tilde{q}} + \Lambda \tilde{q}$$

$$\tau = \hat{M}(q)a + \hat{C}(q, \dot{q})v + \hat{G}(q) - K_G r + \hat{K}q + \hat{D}v \quad (11)$$

where  $\hat{\mathbb{I}}$  parameters define the estimated values of the original parameters in (5), and  $K_G$  and  $\Lambda$  are  $\mathbb{R}^{3\times 3}$  positive definite diagonal matrices where their elements are equal to  $k_a$  and  $\Lambda_{AP}$ , respectively. As suggested previously [22], the most dominant dynamic effects of the system are the stiffness and the damping. Therefore, to compensate for those parameters, an adaptive term is used to provide more robustness for the bound of uncertainties. The uncertainties in the remaining dynamic terms, including gravity, Coriolis, centrifugal and inertial effects, are compensated using a robust term  $-K_G r$ . The reason for using a robust term instead of an adaptive term lies in the simplicity, reducing complexity and eliminating a computationally expensive regressor matrix for uncertainties in the less dominant G, M, and Cterms. In our previous letter [22], C, M, and G were assumed to be accurate; however, in this study, due to the implementation of actuator pairs, uncertainties could exist. In the following section, we show that the proposed approach still maintains sufficient stability in this scenario and the error converges to a small bound. To provide a better form for the stability proof, (11) is reformulated as

$$\tau = \hat{M}(\boldsymbol{q})\boldsymbol{a} + \hat{C}(\boldsymbol{q}, \dot{\boldsymbol{q}})\boldsymbol{v} + \hat{\boldsymbol{G}}(\boldsymbol{q}) - K_G \boldsymbol{r} + Y_p(\boldsymbol{q}, \dot{\boldsymbol{q}}, \boldsymbol{a}, \boldsymbol{v})\hat{\boldsymbol{\theta}}_{\boldsymbol{p}}$$
(12)

where  $Y_p$  represents the regressor matrix for uncertain and varying parameters  $\hat{\theta}_p$ . Due to computational complexity and low effect, the C matrix was assumed to be a  $\mathbb{R}^{3\times3}$  zero matrix, and the  $\hat{M}$  and  $\hat{G}$  are used in the control rule without any adaptation. The only parameters that will be updated are stiffness and damping variables, which are the dominant effects on the system dynamics. The regressor matrix and adaptable parameters are described as follows

$$Y_p = [\operatorname{diag}([q(1), q(2), q(3)]), \operatorname{diag}([v(1), v(2), v(3)])]$$

$$\hat{\boldsymbol{\theta}}_{p} = \left[ \hat{K}_{1}, \hat{K}_{2}, \hat{K}_{3}, \hat{D}_{1}, \hat{D}_{2}, \hat{D}_{3} \right]^{T}, \tag{13}$$

#### B. Stability Proof

Derivation of the stability proof starts with implementing the control rule (12) into (5) without considering the external forces, and by adding and subtracting Ma, Cv and Dv in the left-hand side, providing

$$M\dot{r} + (C + D + K_G)r = \tilde{M}a + \tilde{C}v + \tilde{G} + Y_p\tilde{\theta}_p$$
 (14)

where  $\hat{[}] = \hat{[}] - []$ , is the difference between the estimated parameter and its true value. Defining the Lyapunov function

$$V = \frac{1}{2} \left( \mathbf{r}^T M \mathbf{r} + \tilde{\boldsymbol{\theta}}_{\boldsymbol{p}}^T \Gamma \tilde{\boldsymbol{\theta}}_{\boldsymbol{p}} \right)$$
 (15)

where  $\Gamma$  is defined as a  $\mathbb{R}^{6\times 6}$  positive definite diagonal matrix and the non-zero elements are defined as  $\Gamma(i,i)=\Gamma_k$  and  $\Gamma(i+3,i+3)=\Gamma_D$ .  $\Gamma_K$  and  $\Gamma_D$  are adaptation gains for stiffness and damping coefficients, respectively. By considering the modeling error we define the  $K_G(i,i)$  such that [31]

$$K_G(i,i) \ge \left| \left[ \tilde{M} \boldsymbol{a} + \tilde{C} \boldsymbol{v} + \tilde{G} \right]_i \right| + \eta_i$$
 (16)

where  $\eta_i$  is a strictly positive constant and  $i \in \{1, 2, 3\}$ . Now, by differentiating the Lyapunov function we have

$$\dot{V} = \mathbf{r}^{T} M \dot{\mathbf{r}} + \frac{1}{2} \mathbf{r}^{T} \dot{M} \mathbf{r} + \tilde{\boldsymbol{\theta}}_{p}^{T} \Gamma \dot{\tilde{\boldsymbol{\theta}}}_{p}$$
(17)

By using (14), we obtain

$$\dot{V} = \frac{1}{2} \boldsymbol{r}^{T} \left( \dot{M} - 2 C \right) \boldsymbol{r} - \boldsymbol{r}^{T} (D + K_{G}) \boldsymbol{r} + \boldsymbol{r}^{T} Y_{p} \tilde{\boldsymbol{\theta}}_{p}$$

$$+ \tilde{\boldsymbol{\theta}}_{p}^{T} \Gamma \dot{\tilde{\boldsymbol{\theta}}}_{p} + \boldsymbol{r}^{T} \left( \tilde{M} \boldsymbol{a} + \tilde{C} \boldsymbol{v} + \tilde{\boldsymbol{G}} \right)$$
(18)

Knowing that  $\dot{M}-2\,C$  is skew-symmetric, the term  $r^T(\dot{M}-2\,C)r$  will be zero. It is true that we are considering C as a zero  $\mathbb{R}^{3\times3}$  in the control rule, but the skew-symmetric property of  $\dot{M}-2\,C$  in simple mechanical systems, similar to the dynamic model under consideration, holds. The model uncertainty in  $\dot{C}$  has been considered in  $\tilde{C}$  which due to its minimal effect, relative to  $\dot{M}$ , will be compensated by the robust term. Using the following adaptive rule

$$\dot{\hat{\boldsymbol{\theta}}}_{\boldsymbol{p}} = -\Gamma^{-1} Y_p^T(\boldsymbol{q}, \dot{\boldsymbol{q}}, \boldsymbol{a}, \boldsymbol{v}) \boldsymbol{r}$$
 (19)

and (16), we obtain the following equation

$$\dot{V} < -\boldsymbol{r}^T (\eta + D) \boldsymbol{r} \tag{20}$$

where  $\eta$  is a  $\mathbb{R}^{3\times3}$  diagonal matrix with non-zero elements equal to  $\eta_i$  for  $i\in\{1,2,3\}$ . Since  $\dot{V}$  is negative semi-definite and V is positive definite, we can conclude that  $\boldsymbol{r}$  and  $\tilde{\boldsymbol{\theta}}_{\boldsymbol{p}}$  are bounded. The boundedness in  $\boldsymbol{r}$  also guarantees the boundedness of  $\boldsymbol{q}$  and  $\dot{\boldsymbol{q}}$  since  $\boldsymbol{r}=\dot{\boldsymbol{q}}+\Lambda\tilde{\boldsymbol{q}}$  can be considered as a stable first-order differential equation for  $\tilde{\boldsymbol{q}}$  with the input  $\boldsymbol{r}$ . In addition, since  $\boldsymbol{q}_d$  and  $\dot{\boldsymbol{q}}_d$  are bounded, the boundedness of  $\boldsymbol{q}$  and  $\dot{\boldsymbol{q}}$  will be guaranteed [31]. Now, by using Barbalat's lemma, if we show that  $\ddot{V}$  is bounded we can conclude as  $t\to\infty$ ,  $\dot{V}\to0$ . which will guarantee  $\boldsymbol{r}\to0$  as  $t\to\infty$ . By differentiating  $\dot{V}$  we have

$$\ddot{V} = -\mathbf{r}^T(\eta + D)\dot{\mathbf{r}} \tag{21}$$

Considering (14) and the positive definiteness of M, which guarantees the existence of  $M^{-1}$ , we can conclude that  $\dot{r}$  and therefore  $\ddot{V}$  is bounded [31]. Thus, we can say as  $t \to \infty$ ,  $r \to 0$ , which implies  $\tilde{q}, \dot{\tilde{q}} \to 0$  as  $t \to \infty$ .

It should be noted that our main objective is to control the system to track the desired trajectories while maintaining the stability of the system, which is equivalent to the boundedness of all the signals. The convergence of adaptable parameters to their true value is out of the primary interest, and they only need to remain bounded [26].

# C. Benchmark Controllers: PD Feedback Linearization (PDFL) and Passivity Control (PC)

To highlight the superiority of the proposed adaptive passivity controller, two benchmark controllers are briefly introduced here. We will first consider the widely used PD Feedback linearization controller [22], [30], which is defined as follows

$$\boldsymbol{\tau} = M \left( \ddot{\boldsymbol{q}}_{\boldsymbol{d}} - K_{\boldsymbol{d}} \dot{\tilde{\boldsymbol{q}}} - K_{\boldsymbol{p}} \tilde{\boldsymbol{q}} \right) + C \dot{\boldsymbol{q}} + D \dot{\boldsymbol{q}} + K \boldsymbol{q} + \boldsymbol{G} \quad (22)$$

where  $K_p$  and  $K_d$  are  $\mathbb{R}^{3\times 3}$  positive definite diagonal matrices where their elements are equal to  $k_p$  and  $k_d$  respectively. The second controller is the passivity controller, where the control rule is the same as (11) but without any adaptation and only consists of constant gains [22].

#### V. EXPERIMENTAL STUDY

#### A. Experimental Setup

The experimental setup consists of three proportional pressure regulators (ITV 1031-21N2BL4, SMC Corporation) with embedded pressure sensors for pressurizing the actuators. The valves are connected to a compressor with an output pressure of 70 psi. The control algorithm was implemented on a Simulink xPC target machine that is connected to an analog output board (DAC6703, National Instrument) which provides 0-5 V signal to control the pressure regulators. The encoders' output was measured with a 32-bit counter PCI (CNT32-8 M, Contec). The algorithm, analog outputs, and measurements are executed with a 1KHz sampling rate. An optical camera (MicronTracker, Claronav, Toronto, Canada) was used to measure the robot tip positions at 16 Hz.

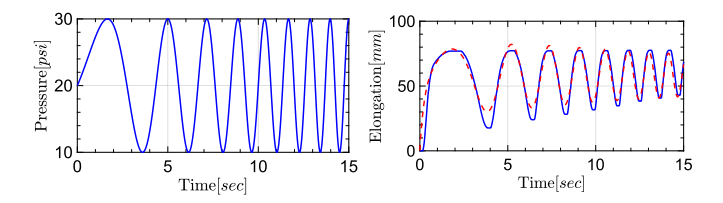


Fig. 3. The left image depicts the input pressure sent to the system. In the right image, the blue shows the measured elongation from the robot and the red is the output from the simulated model in MATLAB.

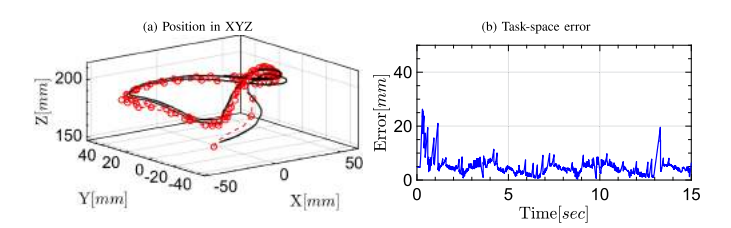


Fig. 4. (Left) End-effector position 3D space. Red indicates the measured results, and black indicates the modeled results. (Right) The end-effector motion error plot.

#### B. System Parameter Identification

System dynamic parameter identification was performed using a chirp signal applied to the regulator of one actuator pair as shown in Fig. 3. Note that parameters may vary between actuator pairs; however, the proposed adaptive control can compensate for these uncertainties. The optimization algorithm is set to constraint nonlinear least square with cost function of sum squared error. The input pressure and system response in simulation and robot hardware are depicted in Fig. 3.

The identified parameters are summarized as follows

$$D = 130.42\mathbf{I}_{3\times3}, \ m = 1.17, \ \alpha_h = 4.78,$$
  
 $K = 538.18\mathbf{I}_{3\times3}, \ \beta_h = 17.67, \ \gamma_h = -68.95$  (23)

where I is the Identity matrix. The variables m, K, and D have units of kg, N/m, and  $N \cdot s/m$ , respectively, and the rest of the parameters are constants.

# C. Kinematic Validation

In this section, we validate the kinematic mapping from actuator-space to task-space. To perform this experiment, each pneumatic muscle actuator is actuated based on a pre-defined signal input. Using the encoder measurements, the task-space end-effector position is calculated and the end-effector position is measured via the stereo camera. The RMSE between the measured value and the modeled value is then evaluated, as shown in Fig. 4. The end-effector error is  $5.06\pm3.25$  mm, which is approximately 3.4% of the robot length. This error is expected to come from imperfect actuator length measurements. However, the overall error is within an acceptable range.

#### D. Dynamic Trajectory Tracking

In this section, the dynamic trajectory tracking performance is investigated. The robot is required to follow a circular path, and the desired actuator variables are defined using closed-form inverse kinematics. To achieve this, first, configuration variables

TABLE I
CONTROL PARAMETERS FOR AP AND PDFL

Parameter	$\Lambda_{AP}$	$k_g$	$k_{p}$	$k_d$	$\Gamma_K$	$\Gamma_D$
Value	8	8	$50^{2}$	100	$1e^{-5}$	$1e^{-2}$

will be calculated based on the desired position [32].

$$\theta = \arctan 2(P_y, P_x), \ \lambda = \frac{P_x^2 + P_y^2 + P_z^2}{2\sqrt{P_x^2 + P_y^2}},$$
 
$$\phi = \arcsin\left(\frac{P_z}{\lambda}\right) \tag{24}$$

Using (24) and the geometrical location of the actuators, the actuator-space variables can be calculated as follows [28]

$$l_i = \left[\lambda - r_k \cos\left(\frac{2\pi}{3}(i-1) - \theta\right)\right]\phi - L_0 \qquad (25)$$

where  $i \in \{1, 2, 3\}$ . To further highlight the performance of the system, the system behavior will be examined with various trajectory frequencies (1 rad/s, 3 rad/s), payloads (200 g and 500 g, and external disturbances. The system is required to follow a circle with a 5 cm radius in the XY plane, written as follows

$$X = 0.05\sin(\omega t), \quad Y = 0.05\cos(\omega t), \quad Z = 0.19$$
 (26)

where X, Y, and Z units are in meters. The control parameters are shown in Table I. It should be noted that all the following experiments are implemented for 60 seconds. All the experiments were recorded and submitted as supplementary materials.

1) Trajectory Tracking With  $\omega=1$  rad/s and 3 rad/s Without Load: First, the system was evaluated using the path (26) and  $\omega=1$  rad/s, where high-frequency dynamics do not significantly impact the system. The results in both the actuator-space and task-space are provided to highlight the system performance. Due to camera sampling limitations (i.e. sampling speed and visual obstructions), the robot end-effector position in the trajectory tracking experiments are calculated based on encoder measurements and forward kinematics.

As can be seen in Fig. 5 first row, the AP and PC present a smooth response with good accuracy. In the AP case, after a fast transient response, where the adaptive parameters are updated, the steady-state response accurately followed the desired trajectory, while the PDFL presents overshoot, and lost performance at different states. To further highlight the difference among these controllers, only the time window between 15-30 seconds has been depicted for actuator space tracking. The remaining figures show the result with a duration of 60 seconds. Since we are using the true parameters, as the results suggested in [22], PC should perform close to AP results, which is proved to be true from our experimental results. After increasing the frequency to  $\omega =$ 3 rad/sec, as depicted in the second row of Fig. 5, the tracking error has increased due to the high-frequency dynamics. However, even at higher speeds, the AP still outperforms the benchmark controllers. In both experimental scenarios, the adaptive terms were plotted in Fig. 5, showing the boundedness of these values and highlighting the robustness of the closed-loop system.

2) Trajectory Tracking With  $\omega=1$  rad/s and 3 rad/s Subjected to a 200 g Payload and External Disturbances: In this section, trajectory tracking was performed with an external load

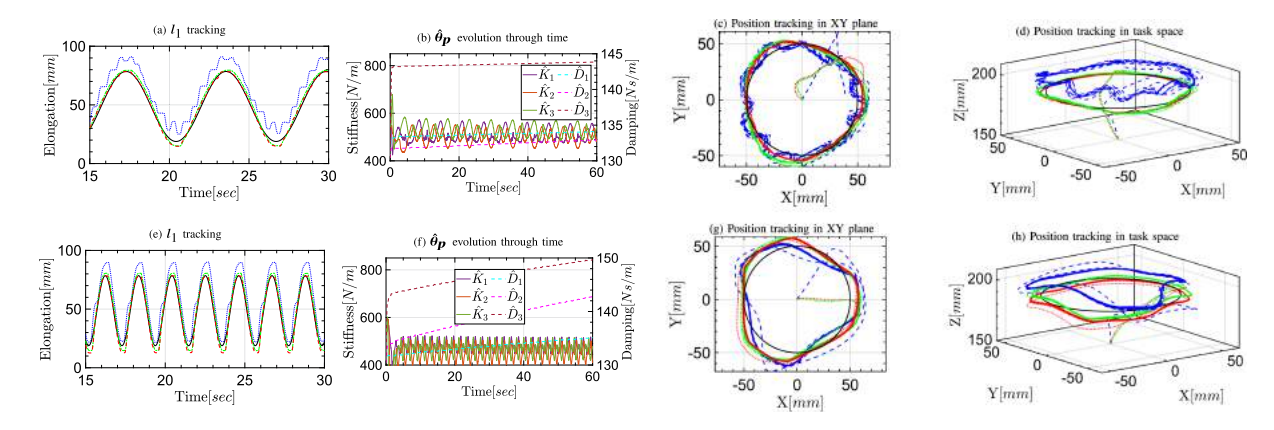


Fig. 5. Trajectory tracking in actuator space and task space along with the evolution of adaptive parameters through time. The AP is in red, PDFL in blue, PC in green, and the desired trajectory in black. The first row represent the results for  $\omega = 1$  rad/s and second row for  $\omega = 3$  rad/s.

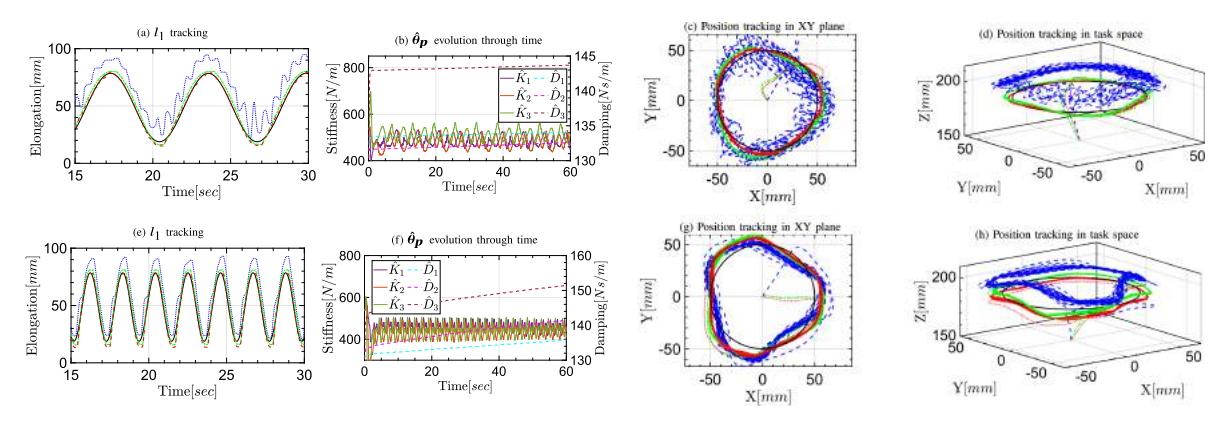


Fig. 6. Trajectory tracking in actuator space and task space along with the evolution of adaptive parameters through time. The AP is in red, PDFL in blue, PC in green, and the desired trajectory in black. The first row represent the results for  $\omega=1$  rad/s and second row for  $\omega=3$  rad/s. The system is subjected to a moving 200 g load.

and unknown disturbance. A 200 g payload is loosely attached to one of the holes on the end plate (refer to the supplementary video). The loose connection style was intentionally chosen such that the load will move in an unpredictable manner during operation, pushing the limit of the controllers by introducing external unknown force with unpredictable directions. The results are depicted in Fig. 6.

As can be seen, both AP and PC maintain their tracking performance while the PDFL presented an oscillatory response, which highlights its poor robustness. This experiment showed the disturbance rejection ability of the proposed AP and PC. To further explore the capability of the AP controller, the speed of the desired path was increased to  $\omega=3$  rad/s. The results are shown in the second row of Fig. 6. As can be seen, similar to the free-space tracking results, as the speed increases, the error bound also increases. However, the AP and PC still retain their stability. It should be noted that the AP controller outperforms the PC which indicates that the AP can compensate for variations in external disturbances. The adaptable parameters remained bounded, which is a strong evidence that in the presence of external disturbance the stability is maintained due to robust+adaptive structure of the proposed AP controller.

3) Trajectory Tracking With the  $\omega=1$  rad/s and 3 rad/s Subjected to a 500 g Payload and External Disturbances: To push the controller limit even further, we increase the 200 g load to 500 g. As can be seen in first row of Fig. 7, the disturbance effect is substantial to the system. However, even in

this situation, the soft robotic hardware, along with the AP controller, maintained stability and outperforms the benchmarks, despite the increased tracking error. It should be noted that lower gains have been used for PDFL in this scenario ( $k_p=30^2$  and  $k_d=60$ ) as the previous gains resulted in instability. To further challenge the controllers, the tracking speed was increased to  $\omega=3$  rad/sec. As can be seen in the second row of Fig. 7, the AP controller achieved the best control performance. The adaptive parameters are also remained bounded in both scenarios which further highlights the robustness of the system.

- 4) Parametric Uncertainty: As we see in previous experiments, the performance of the PC and AP controllers is not far from each other. The reason lies in the accurate modeling and system identification. To highlight the adaptive ability of the AP controller, an additional experiment was been conducted where it has been assumed that the parameters have 50 % inaccuracies. As can be seen in Fig. 8, the AP exhibits superior tracking accuracy with respect to the other controllers. In fact, the adaptive passivity controller shows about 52.4 % improved performance with respect to the passivity controller. The adaptive parameters also remained bounded.
- 5) Disturbance Rejection: To validate the robot's stability, the robot was commanded to follow a desired circular trajectory with  $\omega=1$  rad/sec while an external disturbance with high force in different directions was been exerted onto the system (i.e. prodding the robot). The results are depicted in Fig. 9. As can be seen, all controllers have maintained their

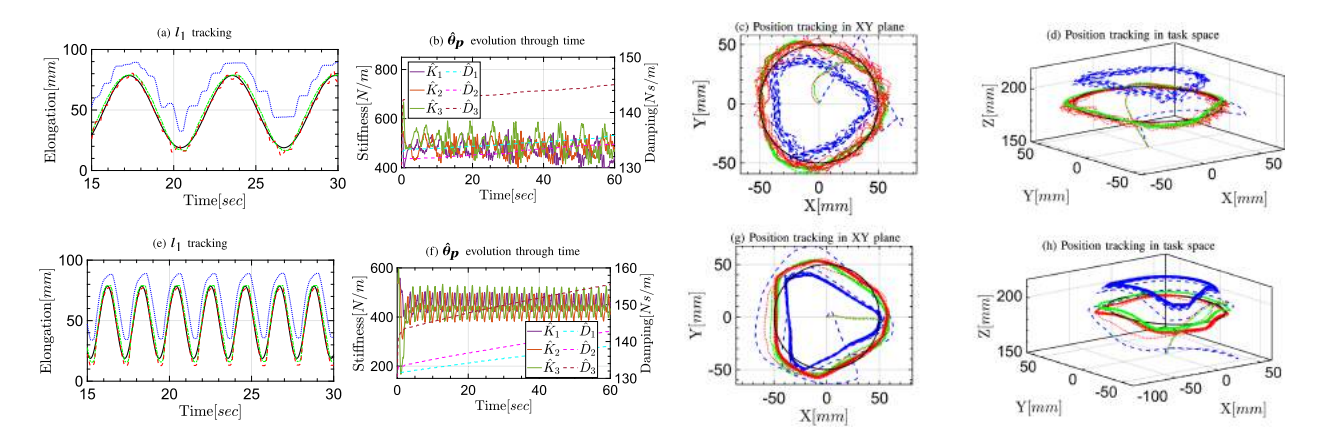


Fig. 7. Trajectory tracking in actuator space and task space along with the evolution of adaptive parameters through time. The AP is in red, PDFL in blue, PC in green, and the desired trajectory in black. The first row represent the results for  $\omega = 1$  rad/s and second row for  $\omega = 3$  rad/s. The system is subjected to a moving 500 g load.

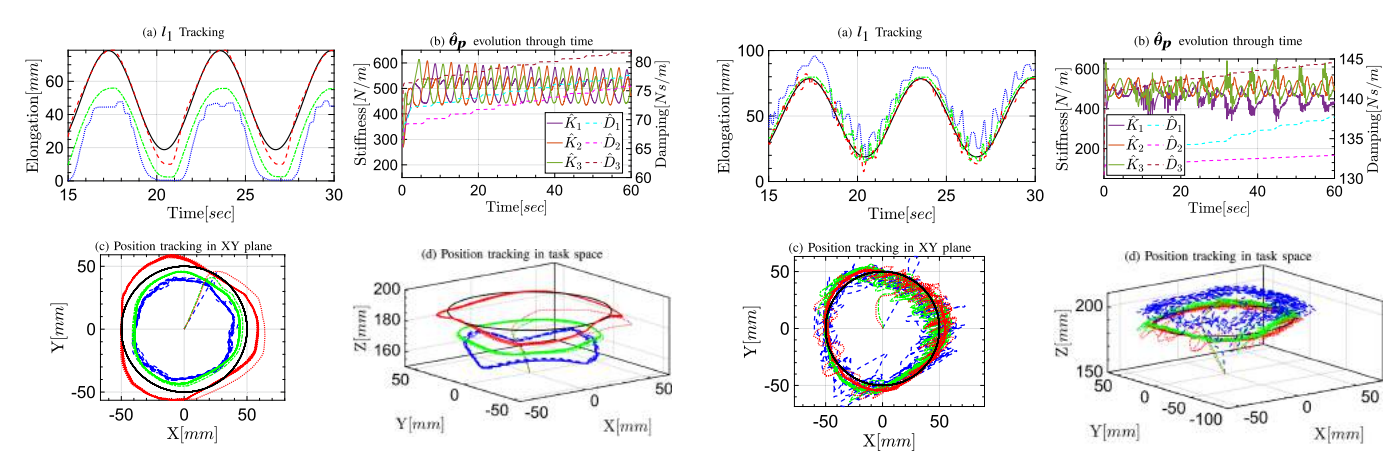


Fig. 8. Trajectory tracking in actuator space and task space along with the evolution of adaptive parameters through time with 50 % uncertainty in stiffness and damping parameters. The AP is in red, PDFL in blue, PC in green, and the desired trajectory in black for  $\omega=1$  rad/s.

Fig. 9. Trajectory tracking in actuator space and task space along with the evolution of adaptive parameters through time in the presence of constant disturbance with different magnitudes and directions. The AP is in red, PDFL in blue, PC in green, and the desired trajectory in black for  $\omega=1$  rad/s.

stability while the AP controller showed superior performance with respect to others by returning to the desired path faster after the disturbance was removed. As we expected, the PC has outperformed the PDFL algorithm, and adaptable parameters remained bounded.

## E. Discussion

To provide a comprehensive overview of the proposed controller in different experimental scenarios described above, we summarize the L2 norm of the error in task-space of the above experiments in Fig. 10 and Table II.

1) Path Speed Effect on Tracking Performance: Based on Fig. 10, it can be seen that the speed will result in reduced tracking accuracy in all the controllers. This can be further highlighted by comparing the mean of the L2 norm error according to Table II. It is obvious that the AP maintained its stability and performance despite the increase of the error, which highlights the robustness and adaptation capabilities. For manipulation purposes, accuracy and consistency are the most important factors, and both can be achieved using our proposed method. It can be argued that tracking accuracy in AP can be potentially improved

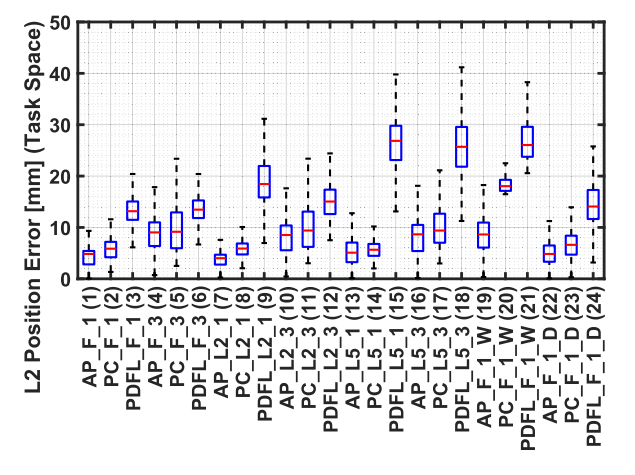


Fig. 10. Boxplot for highlighting the results in different scenarios for AP, PC, and PDFL. The code for the X-Axis from left to right is as follows: [Control Type]-[Free(F) or Loaded (L)][m\*100 g payload]-[Speed of the path in rad/s][W= wrong stiffness and damping parameters, D= Disturbance rejection scenario][Data ID].

Data ID

Mean Error [mm]

Data ID

Mean Error [mm]

Data ID

Mean Error [mm]

BY WHITE ROWS										
Controller	AP	PC	PDFL	AP	PC	PDFL				
Data ID	1	2	3	4	5	6				
Mean Error [mm]	4.73	6.21	13.49	9.01	9.84	13.94				

19.54

15

26.95

21

26.71

10

8.43

16

8.48

22

5.97

11

10.14

17

10.17

23

8.02

12

15.48

18

26.36

24

15.23

TABLE II

18.5 The data ID is highlighted by gray color and is defined in fig. 10 caption.

6.31

14

6.13

20

4.27

13

5.83

19

8.81

with high gain, but it will inevitably increase the chattering and non-smooth behavior of the robot, leading the system to instability due to increasing the aggressiveness of the controller. Alternative strategies for high-speed effects compensation are discussed in Section VI.

2) Disturbance/Payload Effect on Tracking Performance: According to Table II, the mean L2 error for PDFL approach has increased after introducing external load/disturbances into the system. However, the AP and PC, retained their performance and stability, and the results also indicated that the variation was minimal, which highlighted their robustness. It should be mentioned that in all scenarios AP outperformed the PC controller in terms of accuracy.

# VI. CONCLUSION

In this letter, we present the soft robot hardware and encoder design to investigate the control strategy for different operation scenarios. The letter is an extension of our prior theoretical work [22], with new efforts focused on controller stability proof and experimental validations. With the robust hardware prototype, we have experimentally shown that the proposed AP control scheme can maintain its tracking performance in challenging operation scenarios where the classic PDFL or PC strategies typically fail. In our future studies, we plan to address the dynamic control of a multi-section soft robotic arm by designing a controller which can adapt to uncertainties and the probabilistic behavior of the robot. Implementing the probabilistic methods along with adaptive ability could compensate for the uncertainties in a fast and smooth manner, which can result in a more robust and consistent performance at higher speeds that can be crucial for certain industrial applications, such as pick-place tasks.

#### REFERENCES

- [1] C. Laschi, B. Mazzolai, and M. Cianchetti, "Soft robotics: Technologies and systems pushing the boundaries of robot abilities," Sci. Robot., vol. 1, no. 1, 2016, Art. no. eaah3690.
- [2] Y. Chen, L. Wang, K. Galloway, I. Godage, N. Simaan, and E. Barth, "Modal-based kinematics and contact detection of soft robots," Soft Robot., vol. 8, no. 3, pp. 298-309, 2021.
- [3] D. Rus and M. T. Tolley, "Design, fabrication and control of soft robots," Nature, vol. 521, no. 7553, pp. 467-475, 2015.
- [4] J. R. Amend, E. Brown, N. Rodenberg, H. M. Jaeger, and H. Lipson, "A positive pressure universal gripper based on the jamming of granular material," IEEE Trans. Robot., vol. 28, no. 2, pp. 341-350, Apr. 2012.
- D. D. K. Arachchige, Y. Chen, I. D. Walker, and I. S. Godage, "A novel variable stiffness soft robotic gripper," in Proc. IEEE 17th Int. Conf. Automat. Sci. Eng., 2021, pp. 2222-2227.
- Y. Li, Y. Liu, K. Yamazaki, M. Bai, and Y. Chen, "Development of a soft robot based photodynamic therapy for pancreatic cancer," IEEE/ASME Trans. Mechatron., vol. 26, no. 6, pp. 2977-2985, Dec. 2021.

- [7] M. Musa, S. Sengupta, and Y. Chen, "MRI-compatible soft robotic sensing pad for head motion detection," IEEE Robot. Automat. Lett., vol. 7, no. 2, pp. 3632–3639, Apr. 2022.
- [8] M. Pan et al., "Soft actuators and robotic devices for rehabilitation and assistance," Adv. Intell. Syst., vol. 4, no. 4, 2022, Art. no. 2100140.
- A. L. Gunderman, J. A. Collins, A. L. Myers, R. T. Threlfall, and Y. Chen, "Tendon-driven soft robotic gripper for blackberry harvesting," IEEE Robot. Automat. Lett., vol. 7, no. 2, pp. 2652-2659,
- [10] D. D. K. Arachchige, Y. Chen, and I. S. Godage, "Soft robotic snake locomotion: Modeling and experimental assessment," in Proc. IEEE 17th Int. Conf. Automat. Sci. Eng., 2021, pp. 805-810.
- [11] M. S. Xavier et al., "Soft pneumatic actuators: A review of design, fabrication, modeling, sensing, control and applications," IEEE Access, vol. 10, pp. 59442-59485, 2022.
- [12] J. Till, V. Aloi, and C. Rucker, "Real-time dynamics of soft and continuum robots based on Cosserat rod models," Int. J. Robot. Res., vol. 38, no. 6, pp. 723-746, 2019.
- F. Renda, M. Giorelli, M. Calisti, M. Cianchetti, and C. Laschi, "Dynamic model of a multibending soft robot arm driven by cables," IEEE Trans. Robot., vol. 30, no. 5, pp. 1109-1122, Oct. 2014.
- [14] P. Polygerinos et al., "Modeling of soft fiber-reinforced bending actuators," IEEE Trans. Robot., vol. 31, no. 3, pp. 778-789, Jun. 2015.
- [15] F. Largilliere, V. Verona, E. Coevoet, M. Sanz-Lopez, J. Dequidt, and C. Duriez, "Real-time control of soft-robots using asynchronous finite element modeling," in Proc. IEEE Int. Conf. Robot. Automat., 2015, pp. 2550-2555.
- [16] A. A. Algumsan, S. Khoo, and M. Norton, "Robust control of continuum robots using Cosserat rod theory," Mechanism Mach. Theory, vol. 131, pp. 48-61, 2019.
- [17] I. S. Godage, G. A. Medrano-Cerda, D. T. Branson, E. Guglielmino, and D. G. Caldwell, "Dynamics for variable length multisection continuum arms," Int. J. Robot. Res., vol. 35, no. 6, pp. 695–722, 2016.
- [18] I. S. Godage, R. Wirz, I. D. Walker, and R. J. Webster III, "Accurate and efficient dynamics for variable-length continuum arms: A center of gravity approach," Soft Robot., vol. 2, no. 3, pp. 96-106, 2015.
- [19] M. Azizkhani, M. Zareinejad, and M. A. Khosravi, "Model reference adaptive control of a soft bending actuator with input constraints and parametric uncertainties," Mechatronics, vol. 84, 2022, Art. no. 102800.
- [20] I. S. Godage, Y. Chen, and I. D. Walker, "Dynamic control of pneumatic muscle actuators," 2018, arXiv:1811.04991.
- M. S. Xavier, A. J. Fleming, and Y. K. Yong, "Nonlinear estimation and control of bending soft pneumatic actuators using feedback linearization and UKF," IEEE/ASME Trans. Mechatron., vol. 27, no. 4, pp. 1919-1927, Aug. 2022.
- [22] M. Azizkhani, I. S. Godage, and Y. Chen, "Dynamic control of soft robotic arm: A simulation study," IEEE Robot. Automat. Lett., vol. 7, no. 2, pp. 3584-3591, Apr. 2022.
- [23] C. D. Santina, R. K. Katzschmann, A. Bicchi, and D. Rus, "Model-based dynamic feedback control of a planar soft robot: Trajectory tracking and interaction with the environment," Int. J. Robot. Res., vol. 39, no. 4, pp. 490-513, 2020.
- V. Falkenhahn, A. Hildebrandt, R. Neumann, and O. Sawodny, "Dynamic control of the bionic handling assistant," IEEE/ASME Trans. Mechatron., vol. 22, no. 1, pp. 6-17, Feb. 2017.
- [25] M. Trumić, C. D. Santina, K. Jovanović, and A. Fagiolini, "Adaptive control of soft robots based on an enhanced 3D augmented rigid robot matching," in Proc. IEEE Amer. Control Conf., 2021, pp. 4991-4996.
- [26] J.-J. E. Slotine and W. Li, "On the adaptive control of robot manipulators," Int. J. Robot. Res., vol. 6, no. 3, pp. 49-59, 1987.
- A. Kazemipour, O. Fischer, Y. Toshimitsu, K. W. Wong, and R. K. Katzschmann, "Adaptive dynamic sliding mode control of soft continuum manipulators," in Proc. IEEE Int. Conf. Robot. Automat., 2022, pp. 3259-3265.
- [28] I. S. Godage, G. A. Medrano-Cerda, D. T. Branson, E. Guglielmino, and D. G. Caldwell, "Modal kinematics for multisection continuum arms," Bioinspiration Biomimetics, vol. 10, no. 3, 2015, Art. no. 035002.
- [29] I. S. Godage, D. T. Branson, E. Guglielmino, and D. G. Caldwell, "Pneumatic muscle actuated continuum arms: Modelling and experimental assessment," in Proc. IEEE Int. Conf. Robot. Automat., 2012, pp. 4980-4985.
- [30] M. W. Spong and M. Vidyasagar, Robot Dynamics and Control. Hoboken, NJ, USA: Wiley, 2008.
- [31] J.-J. E. Slotine and W. Li, Applied Nonlinear Control, vol. 199. Englewood Cliffs, NJ, USA: Prentice-Hall, 1991.
- S. Neppalli, M. A. Csencsits, B. A. Jones, and I. D. Walker, "Closedform inverse kinematics for continuum manipulators," Adv. Robot., vol. 23, no. 15, pp. 2077-2091, 2009.